Applied Thermal Engineering 259 (2025) 124756

Contents lists available at ScienceDirect

Applied Thermal Engineering

journal homepage: www.elsevier.com/locate/apthermeng

Research Paper

# Experimental study on the effect of an ionic liquid as anti-crystallization additive in a bi-adiabatic $H_2O$-LiBr absorption chiller prototype

Hussain A. Tariq [a], Amín Altamirano [b], Romain Collignon [c], Benoit Stutz [c,*], Alberto Coronas [a,*]

[a] CREVER - Group of Applied Thermal Engineering, Department of Mechanical Engineering, Universitat Rovira i Virgili, Av. Països Catalans 26, Tarragona 43007, Spain
[b] Laboratoire du froid et des systèmes énergétiques et thermiques (Lafset), Conservatoire national des arts et métiers, Paris F 75003, France
[c] Univ. Savoie Mont Blanc, CNRS, LOCIE, Chambéry 73000, France

ARTICLE INFO

*Keywords:*
Absorption chiller
Heat and mass transfer
Ionic liquid
[DMIM][Cl]
Additive
$H_2O$-LiBr

ABSTRACT

Absorption chillers are attractive because they use natural refrigerants and can be powered by low-grade heat sources. Among the commercially available working fluids, the most common one, $H_2O$-LiBr, has a critical drawback associated with the crystallization of the solution at low temperatures and high absorbent concentrations. This limitation restricts the operating range of these systems, especially when they are air-cooled or used as heat pumps. Additives can be used in $H_2O$-LiBr to reduce the crystallization temperature by improving the solubility of LiBr in the solution. However, they often present disadvantages such as the requirement of a rectifier, and a negative impact on heat and mass transfer. Ionic Liquids (ILs) used as additives represent an alternative to overcome these drawbacks. In the present study, 6 % of [DMIM][Cl] by mass in absorbent (LiBr + [DMIM][Cl]) is added as an anti-crystallization additive to study its effect on the experimental behavior and crystallization limit of a $H_2O$-LiBr single-effect bi-adiabatic absorption chiller prototype. Results of $H_2O$-LiBr and $H_2O$–(LiBr + [DMIM][Cl]) were compared for the individual heat transfer elements and the global system COP. The results show a decrease in the crystallization temperature using $H_2O$–(LiBr + [DMIM][Cl]), which extended the operating range of the prototype. A decrease of 15 °C in crystallization temperature was found for $H_2O$–(LiBr + [DMIM][Cl]) compared to $H_2O$-LiBr at an absorbent mass of 65 %. Crystallization impeded the operation for $H_2O$-LiBr at the highest driving temperature (100 °C) and lowest cold source inlet temperature (9 °C), whereas no crystallization was observed at same operating conditions for the (LiBr + [DMIM][Cl]) solution. Under the tested conditions, the addition of the IL as additive increased the chiller operating range without the requirement of a rectifier and with a negligible impact on the cooling capacity and thermal COP.

## 1. Introduction

The demand of cooling, particularly in warmer regions, is rising due to population growth, improved living standards, and global warming. This trend is driving increased demand for air conditioning, with projections indicating a tripling of demand from 2016 to 2050 [1]. Currently, space cooling accounts for 3 % of global primary energy consumption [2], largely reliant on electric vapor compression technology [3]. However, this technology faces environmental challenges due to high electricity consumption and greenhouse gas emissions from synthetic refrigerants, which cause global warming. To address these challenges, sustainable cooling technologies are crucial. Absorption chillers offer a promising alternative, utilizing natural refrigerants and capable of being powered by waste heat or any low-grade heat sources (ideally, renewable). Their implementation can help reduce electricity consumption, greenhouse gas emissions, and other environmental impacts associated with cooling systems [4 5 6].

Various working pairs have been suggested for absorption technology [7], but many have been deemed unsuitable due to factors such as explosion risks, high costs, corrosion, environmental hazards, inadequate transport properties, and chemical instability. Ammonia-water ($NH_3$-$H_2O$) is commonly used (ammonia is used as refrigerant and water as absorbent) [8 9], but it requires higher driving temperatures and an additional component, the rectifier. Ammonia's toxicity also limits its suitability for space heating and cooling, as inhalation of low concentrations of ammonia can cause coughing, irritation of the nose and throat, while higher concentrations can lead to severe lungs damage or fatality [10]. Water-Lithium Bromide ($H_2O$-LiBr) is preferred for its high efficiency, non-toxicity, no need of a rectifier, and low cut-off temperatures [11 7]. In this solution, water is used as a refrigerant which is abundant, non-toxic, and inexpensive, while LiBr serves as an

* Corresponding authors.

https://doi.org/10.1016/j.applthermaleng.2024.124756
Received 19 April 2024; Received in revised form 17 October 2024; Accepted 28 October 2024
Available online 2 November 2024
1359-4311/© 2024 The Authors. Published by Elsevier Ltd. This is an open access article under the CC BY license (http://creativecommons.org/licenses/by/4.0/).

**Nomenclature**

| | |
|---|---|
| COP | Coefficient of Performance |
| $C_p$ | Specific Heat, $kJ.kg^{-1}.K^{-1}$ |
| C | Heat capacity, $W.K^{-1}$ |
| IL | Ionic Liquid |
| k | Thermal conductivity, $W•m^{-1}•K^{-1}$ |
| LiBr | Lithium Bromide |
| $\dot{m}$ | mass flow rate, $kg.s^{-1}$ |
| $\dot{Q}$ | Heat load |
| T | temperature, °C/K |
| $\rho$ | density, $kg.m^{-3}$ |
| p | Pressure, kPa |
| $\mu$ | Dynamic viscosity, mPa•s |
| ε | Thermal effectiveness of heat exchangers |
| [DMIM][Cl] | 1,3-dimethylimidazolium chloride |

*Subscripts and superscripts*

| | |
|---|---|
| a | absorber |
| act | actual |
| c | condenser |
| c.sol | concentrated solution |
| d | desorber |
| d.sol | diluted solution |
| Dis | Distributor |
| e | evaporator |
| EG | Ethylene Glycol (50 %) based water solution |
| ext | external circuit |
| htf | heat transfer fluid |
| i | inlet |
| max | maximum |
| o | outlet |
| Res | Reservoir |
| SHX | solution heat exchanger |
| th | thermal |
| wt | liquid water |
| w | mass fraction |

absorbent. Although there are some obstacles using this solution (e.g., it is highly corrosive, it requires bulky components and it presents high initial cost), but its benefits generally overshadow the drawbacks. Nevertheless, LiBr crystallization at high concentrations hinders its operating range and complicates its implementation in air-cooled systems and heat pumps (for heating purposes). In this case, a separate direct-contact cooling tower for heat dissipation becomes necessary to set the intermediate temperature below the ambient temperature, which in consequence increases the overall system cost and size. Furthermore, cooling towers are associated with respiratory infections risks caused by Legionella bacteria. Therefore, improving the solubility of LiBr in the $H_2O$-LiBr solution can enable the technology to be air cooled, eliminating the need of a cooling tower. Furthermore, air cooled systems offer several benefits including reduced maintenance, lower operating costs and a compact size.

In recent years, researchers have addressed LiBr crystallization issues through various methods, including thermodynamic cycle modifications, system control strategies, improvements in the heat and mass transfer processes, and crystallization inhibitors [16]. Regarding the first method, Izquierdo et al. [12] performed a comparative simulation study of single and double-effect absorption cycle to examine the limitations of air-cooled absorption systems due to the crystallization of LiBr in $H_2O$-LiBr. Crystallization impedes the operation of the single-effect cycle when the condensing temperature exceeds 40 °C. However, the double-effect cycle can operate at condensing temperatures up to 53 °C. Regarding the second method, Liao and Radermacher [13] investigated temperature control strategies to prevent crystallization in air-cooled absorption chillers, enabling their use in cooling, heating, and power systems. However, this innovative approach compromises the cooling capacity and COP of the absorption chiller. Finally, regarding the third and fourth methods, Reimann et al. [14] prepared a solution called "Carrol" which contains LiBr, ethylene glycol, and 1-nonylamine. In this solution, 1-nonylamine is used as an additive to improve heat and mass transfer, while ethylene glycol acts as a crystallization inhibitor. It was found that the film heat transfer coefficient increased by around 100 %. However, 1-nonylamine was later replaced by phenylmethyl carbinol due to its side effect of forming chemically refractory copper soaps in the presence of copper oxide upon heating. A comparison of the crystallization curves between Carrol and $H_2O$-LiBr revealed that Carrol offers a larger feasible operational area than $H_2O$-LiBr. However, due to the potential presence of trace amounts of ethylene glycol in the vaporized refrigerant from the generator, Inoue [15] and Park et al. [16] recommended incorporating a rectifier in absorption systems utilizing Carrol as the working fluid. Kim et al. [17] analyzed the theoretical COP of LiBr + $H_2N(CH_2)_2OH$ + $H_2O$, LiBr + $HO(CH_2)_3OH$ + $H_2O$ and LiBr+ $(HOCH_2CH_2)_2NH$ + $H_2O$ as potential working fluid solutions for air-cooled absorption chillers. Among these solutions, LiBr + $H_2N(CH_2)_2OH$ + $H_2O$ provided the widest operating range due to its improved solubility. However, several problems were identified, including corrosion, deterioration of heat and mass transfer performance, and the requirement of a rectifier. Yoon and Kwon [18] performed a cycle analysis of an air-cooled double-effect absorption chiller using $H_2O$-LiBr + 1,3 propanediol ($HO(CH_2)_3OH$) as a new working fluid. The simulation results indicated that this new working fluid could offer an 8 % higher crystallization limit compared to the conventional $H_2O$-LiBr solution. Thermal properties and corrosion characteristics of $LiNO_3$ in $H_2O$-LiBr, LiI in $H_2O$-LiBr [19], and (LiI + $LiNO_3$ + LiCl) in $H_2O$-LiBr [20] were reported. $LiNO_3$ was added as a crystallization inhibitor and corrosion inhibitor. Likewise, LiI also acts as a crystallization inhibitor, while LiCl acts as a pressure depletion agent. Different proportions and combinations of (LiCl + LiI + $LiNO_3$) in $H_2O$-LiBr were then used by a Japanese company [21] for a double effect air-cooled absorption machine. As a result, the allowable operating temperature for condenser and absorber increases by 4 °C and 10 °C, respectively, compared to a water-cooled system. In a systematic investigation, Wang et al. [22] examined the crystallization temperature of $H_2O$–(LiBr + $CHO_2Na$). The results showed an unsatisfactory crystallization performance of the proposed solution, complicating its implementation in a refrigeration system.

In the search for new absorbents for the conventional refrigerants ($NH_3$ and $H_2O$) to form innovative working fluids that overcome the drawbacks of the conventional working fluids, Ionic liquids (ILs), liquid-state salts at room temperature, have gained attention in absorption technology. Araújo et al. [23] performed a thermodynamic analysis of a single-effect absorption refrigeration system using two ILs as absorbents ([EMIM][$EtSO_4$] and [EMIM][$BF_4$]). The $H_2O$–[EMIM][$EtSO_4$] solution showed similar COP and an exergetic efficiency compared to conventional $H_2O$-LiBr systems, especially at low absorber and condenser temperatures and high evaporator temperatures. Zhai et al. [24] explored five different ILs ([BMIM][BF4], [DMIM][DMP], [EMIM][DMP], [EMIM][OAc], and [EMIM][OMs]) under different operating conditions, finding LiBr optimal for a targeted COP below 0.778. On the other hand, [EMIM][OAc], [EMIM][OMs], and [BMIM][$BF_4$] exhibited a superior performance for a targeted COP above 0.778. Despite theoretical good performances and no crystallization issues, ILs' poor transport properties result in lower experimental thermal COPs.

Alternatively, ILs have recently been suggested as additives for $H_2O$-LiBr given their low vapor pressure and water absorption capabilities [25 26 27]. Their implementation could provide an anti-crystallization effect without the common drawbacks associated with commonly known additives (the requirement of a rectifier, and a negative impact on heat and mass transfer). Królikowska et al. [28 29] investigated various ILs' influence on the solubility of $H_2O$-LiBr. They concluded that even small quantities of IL significantly affect the range of liquid composition achievable at the operating temperature conditions of the absorber. Shiflett et al. [30] studied various ionic compounds in $H_2O$-LiBr and found them to be effective as working solutions in absorption systems. The inclusion of these ionic compounds as additives demonstrated a reduction in the crystallization issue in such systems.

Absorption chillers are attractive because they utilize natural refrigerants and can be powered by waste heat or other low-grade heat sources. The $H_2O$-LiBr working solution is preferred due to its non-toxicity, the absence of a need for a rectifier, and its low cut-off temperatures. However, the inherent crystallization issue of LiBr makes this technology difficult to operate at high concentrations. Implementing ILs as additives enhances LiBr solubility in $H_2O$-LiBr, facilitating the use of absorption machines as air-cooled systems and heat pumps. Despite some research indicating this potential, there is a gap in the literature regarding the impact of ILs as an additive on real prototypes. This study aims to address this gap by investigating the effect of adding an IL as additive in a $H_2O$-LiBr single-stage bi-adiabatic absorption chiller that uses a technology patented by Altamirano Cundapí et al. [31]. After the most promising additive was identified ([DMIM][Cl]), it was added as part of the absorbent in $H_2O$-LiBr and incorporated into the prototype. Results compare the behavior of the different heat transfer elements and the overall prototype performances using both $H_2O$-LiBr and $H_2O$–(LiBr + [DMIM][Cl]).

## 2. Methodology

In order to meet the above-mentioned objectives, the following methodology is adopted: the selection of the most promising additive and the preparation of the $H_2O$–(LiBr + [DMIM][Cl]) solution are discussed in detail in section 2.1. The thermophysical properties of [DMIM][Cl] in $H_2O$-LiBr is discussed in section 2.2. The description of the absorption machine prototype and experimental conditions employed for this study are discussed in section 2.3. Finally, the procedure to evaluate the data is described in section 2.4.

### 2.1. Selection of ionic liquid and solution preparation

In the process of choosing the most promising commercial ionic liquid to be used as an additive, two key properties were taken into consideration: first, the reduction in crystallization temperature with respect to the pure $H_2O$-LiBr solution and second, a vapor pressure close to that of $H_2O$-LiBr. Based on this, five different ILs were selected: 1,3-dimethylimidazolium chloride [DMIM][Cl], 1-Butyl-3-methylimidazolium bromide [BMIM][Br], 1-Butyl-3-methylimidazolium chloride [BMIM][Cl], Tris-(2-hydroxyethyl)-methyl-ammonium methyl sulfate $[MN((CH_2)_2(OH))_3][MeSO_4]$ and 1-Butyl-3-methylimidazolium acetate [BMIM][OAc] after literature review [32 30]. Their chemical and physical properties were characterized, as this was crucial for accurately determining their thermophysical properties. Since the chemicals were provided by various companies, it was essential to verify their chemical structures and identify present impurities. Nuclear Magnetic Resonance (NMR) Spectroscopy was used to verify the chemical structure of each IL. Only small peaks were observed, which can correspond to some remaining products from the synthesis process. The presence of impurities such as water and halides were assessed through titration and atomic absorption spectroscopy methods. The water content of ILs ranged from 200 to 6500 ppm, which was satisfactory given their strong hydrophilic nature, making water removal a challenging task. Whereas the halide content in each IL was below 200 ppm, aligning with the specifications provided by the supplier companies. The thermal stability of the ILs was measured using a thermogravimetric balance, indicating that each selected IL exhibits a stability above 200 °C. The $[MN((CH_2)_2(OH))_3][MeSO_4]$ was discarded because it presented some side reactions with the LiBr.

To determine the minimal amount of ionic liquid (IL) necessary to achieve a substantial decrease in crystallization temperature (more than 10 °C), the solubility temperature was measured at a total absorbent composition of 65 % (LiBr + IL) for each of the ILs solution. The solubility temperature was obtained when the last crystal disappears upon heating the solution. The IL mass fraction in the absorbent was raised from 0 % to 33 %, increasing by 3 % approximately at each step. From the tested ILs solutions, the one with [DMIM][Cl] shows the solubility temperature depletion of more than 10 °C for a 6 % mass fraction in absorbent, whereas the other solutions required 9 % mass fraction of additive to reach similar results. At 6 % mass fraction of ILs in absorbent, the decrease in crystallization temperature follows this order: [DMIM][Cl] > [BMIM][OAc] > [BMIM][Cl] > [BMIM][Br].

Another important criterion in selecting the ionic liquid was the vapor pressure of the resultant working solution. A working solution with lower vapor pressure is important because it indicates a stronger affinity between water and the absorbent. For this, the vapor pressure of the ILs (with mass fraction of 6 % for [DMIM][Cl] while 9 % for [BMIM][OAc], [BMIM][Cl] and [BMIM][Br]) in $H_2O$-LiBr solution was measured. Experimental results showed that for imidazolium based ILs with the same cation, the depletion in vapor pressure has the following order: [Br] > [Cl] > [OAc]. Whereas the reduction of alkyl chain length in the cation results in higher depletion in vapor pressure of the system. For the chloride anion, the trend in terms of cation has the following order: [DMIM] > [BMIM]. The vapor pressure values were also compared to those obtained by Raoult's law, corresponding to the partial vapor pressure of water, as the absorbent was considered non-volatile. The four IL solutions show a negative deviation from the values calculated by Raoult's law at 30 °C, signifying a strong affinity between the refrigerant and the absorbent. Among all the investigated $H_2O$–(LiBr + IL) solutions, $H_2O$–(LiBr + [DMIM][Cl]) presents vapor pressure closer to the $H_2O$-LiBr solution.

Based on solubility and vapor pressure, [DMIM][Cl] with a mass fraction of 6 % in absorbent (LiBr + IL) was selected. Further details on the selection and composition of the Ionic Liquid are provided in an internal report of the CREVER Research Group that is result of a collaborative work with YTC America [33].

To examine the thermal stability of new solution H2O–(LiBr + [DMIM][Cl]), the sample was prepared in glass vessel and stirred for 30 min. It was distributed to two closed vessels where one sample was kept at room temperature while the other one was kept in an oven at 95 °C. The pH and NMR spectra was performed on the prepared samples after 14 days. It was found that the pH and structure of samples does not show significant changes comparing to the spectrum of freshly prepared sample. After 32 days, the experiments were repeated and found NMR spectra similar to the sample prepared after 14 days. The pH was approximately similar (little less) as compared to the sample prepared after 14 days. Finally, to prepare the solution, [DMIM][Cl] with 97 % of purity was added as an additive in $H_2O$-LiBr. In the absorbent (LiBr + [DMIM][Cl]), the mass fraction of 6 % is attributed to [DMIM][Cl] while remaining 94 % consist of LiBr. The addition process was carried out with continuous stirring to create a uniformly mixed solution of $H_2O$–(LiBr + [DMIM][Cl]).

The refrigerant used in the $H_2O$–(LiBr + [DMIM][Cl]) solution is $H_2O$, a natural refrigerant that is safe and poses no harm for space cooling and heating applications. While LiBr and [DMIM][Cl] are non-volatile, chemically and thermally stable, making them suitable for use in absorption refrigeration systems. Additionally, they are non-flammable, reducing the risk of fire-related incidents. Although they are non-volatile, but they are toxic. Careful handling and disposal are

recommended to minimize adverse effects on health and the environment. The use of appropriate personal protective equipment is advised when handling LiBr and [DMIM][Cl]. In case of skin or eye exposure, rinsing with plenty of water is recommended. Therefore, the addition of [DMIM][Cl] does not pose any significant additional safety or environmental risks compared to LiBr.

### 2.2. Thermophysical properties of the $H_2O$–(LiBr + [DMIM][Cl]) solution

The properties of $H_2O$-LiBr containing 6 % of [DMIM][Cl] as additive in absorbent were experimentally determined by the CREVER Research Group. The visual-polythermal method was used to measure the solubility; this method involves identifying the temperature at which the transition from a solid to a liquid phase occurs, i.e., when the last crystal dissolves in a saturated solution. The procedure conducted with the use of a glass cell and thermal bath. The cell's temperature was measured using a digital precision thermometer (Anton Paar MKT100) equipped with a platinum thermoresistance PT 100 with the accuracy of ± 0.01 K. The estimated uncertainty in the experimental temperature was ± 0.02 K. The detailed experimental technique is described in reference [34]. The solubility data of $H_2O$-LiBr and $H_2O$–(LiBr + [DMIM][Cl]) for absorbent mass fractions ($w_{abs} = w_{IL} + w_{LiBr}$) from 57 % to 69 % corresponding to temperatures from 0 to 90 °C is presented in Fig. 1 [34 35]. From this figure, one can observe that the solubility limit at similar absorbent concentrations is reached for lower solution temperatures in the case of the solution with the additive, which clearly decreases the risk of crystallization of the solution if implemented in an absorption chiller prototype.

A static method was used to obtain the vapor pressure data. The experimental method and apparatus detail is described in reference [36]. The setup included an equilibrium cell, a precise pressure controller (Ruska), a differential pressure null transducer (DPT) (Ruska) and two Haake proportional temperature controllers for a double walled thermostated bath of 25 L capacity filled with water. The bath temperature was controlled (within ± 0.01 K) and determined utilizing a digital precision thermometer (Anton Paar MKT 100). Two stainless steel cells (with volumes of 149 $cm^3$ and 193 $cm^3$) were used for high-pressure measurements. Pressure was measured using digital pressure gauges (with uncertainty of ± 0.05 kPa). Mettler balance (with a precision of ± 0.001 g) was used to weigh the components. Fig. 2 shows the vapor pressure for an absorbent mass fraction between 52.31 % to 62.24 %, corresponding to solution temperatures in the range of 20 °C to 100 °C. Even though the vapor pressure lines at identical concentration are close to each other, as a general trend, one can observe that the vapor pressure of the $H_2O$–(LiBr + [DMIM][Cl]) solution is higher than that of the $H_2O$-LiBr solution. This would lead to slightly higher equilibrium absorbent concentrations in an experimental prototype given the same pressure and temperature conditions in the sorption exchangers (i.e., the absorber and the desorber). The combined uncertainties in vapor pressure were ± 0.037 kPa (when p ≤ 10 kPa), ±0.14 kPa (when p ≤ 20 kPa), and ± 0.12 kPa (p ≤ 50 kPa), where uncertainty in absorbent mass fraction and temperature were 0.02 %, and 0.1 K respectively, with a 95 % level of confidence (k = 2).

An Anton-Paar vibrating tube densimeter connected to pressure system was used to obtain the density. To avoid the evaporation of the solvent, pressure was set higher than the saturation level across the entire measurement range. The vibrating tube densimeter was temperature-controlled using a water bath with a resolution of 0.1 K. A digital precision thermometer (Anton Paar MKT100) with ± 0.01 K accuracy was used to measure the sample temperatures. The experimental setup and procedure have been previously detailed in ref [37]. Fig. 3 shows the density for absorbent mass fractions from 51.55 % to 61.31 %, corresponding to solution temperatures from 20 °C to 100 °C. As observed from this figure, the density of the proposed solution (with the additive) is systematically lower as compared to the conventional $H_2O$-LiBr solution, which is beneficial to the pressure losses when implemented in an experimental prototype. The maximum difference is noted 6 % on average at 57.14 % mass fraction. It can also be seen that density decreases as the mass fraction decreases and temperature increases. The combined uncertainty in density was 1.1 kg•$m^{-3}$, where uncertainties in mass fraction and temperature were 0.02 % and 0.1 K respectively, with a 95 % level of confidence (k = 2).

A piston-type viscometer (Cambridge Viscopro 2000) was utilized (viscosity range of 1 to 20 mPa·s). The measurements were temperature-controlled using a Julabo F20-ME water bath. To measure the temperature, Pt-100 thermometer situated inside the viscosimeter was used. The more detail about experimental procedure and setup are given in reference [37]. Fig. 4 presents the dynamic viscosity data for absorbent mass fractions from 52.31 % to 62.24 % corresponding to solution temperatures from 30 °C to 100 °C. From this figure, one can observe that the dynamic viscosity of $H_2O$–(LiBr + [DMIM][Cl]) is lower as compared with the $H_2O$-LiBr solution, especially at high absorbent concentrations. It can also be seen that the viscosity decreases as the mass fraction decreases and temperature increases. The maximum difference was noted at the absorbent mass fraction of 57.41 %. The combined uncertainties in dynamic viscosity were ± 7 % (η ≤ 5 mPa•s) and ± 5 % (η ≤ 25 mPa•s), while the uncertainties in mass fraction and

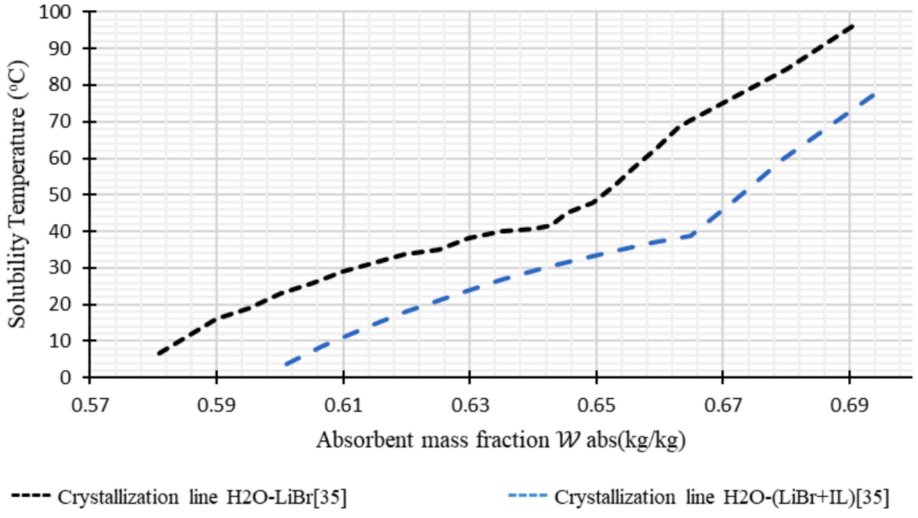


**Fig. 1.** Solid-liquid equilibrium curves of $H_2O$-LiBr and $H_2O$–(LiBr + [DMIM][Cl]) solutions [35].

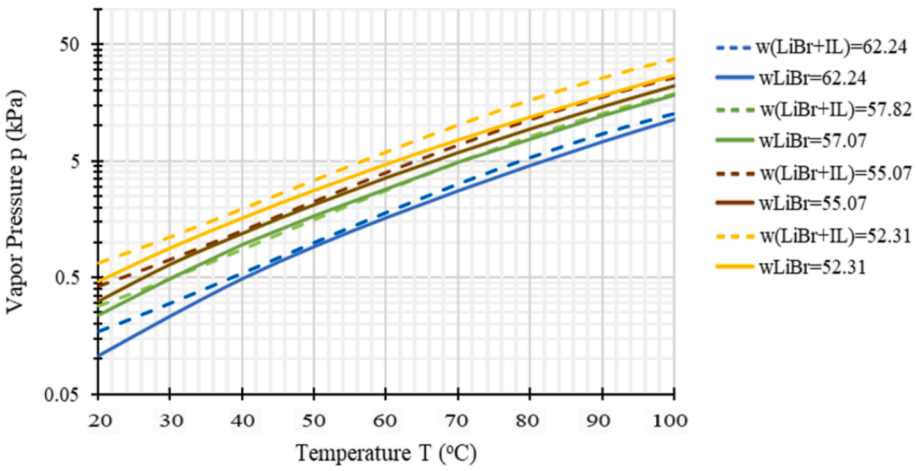


**Fig. 2.** Vapor pressure for $H_2O$–(LiBr + [DMIM][Cl]) and $H_2O$-LiBr at different temperatures and absorbent concentrations [33].

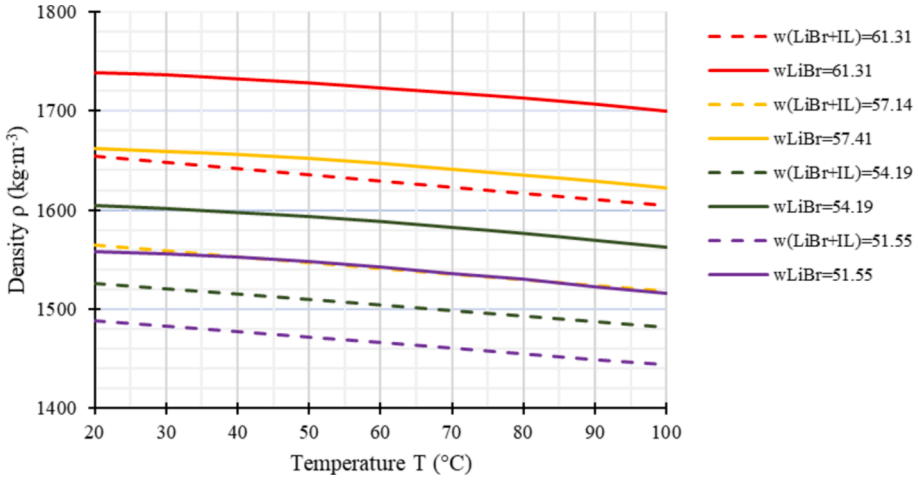


**Fig. 3.** Density of $H_2O$–(LiBr + [DMIM][Cl]) and $H_2O$-LiBr at different temperatures and absorbent concentrations [33].

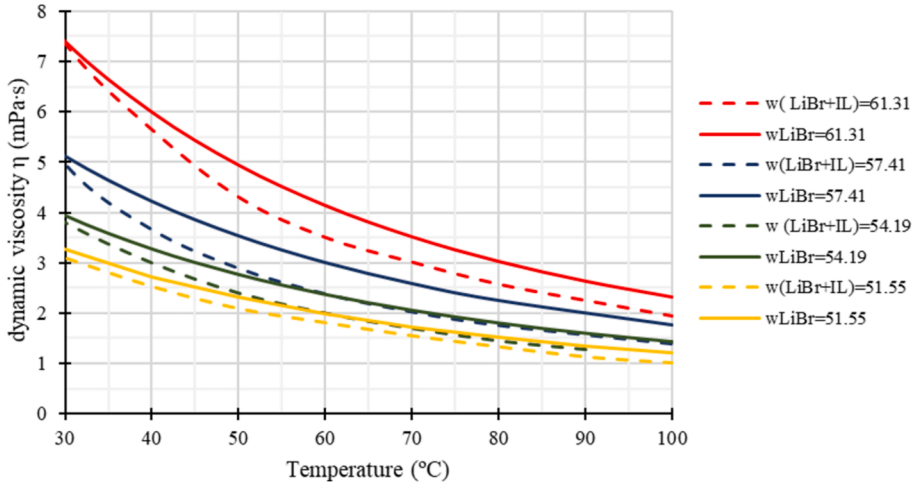


**Fig. 4.** Dynamic viscosity of $H_2O$–(LiBr + [DMIM][Cl]) and $H_2O$-LiBr at different temperatures and absorbent concentrations [33].

temperature were 0.02 % and 0.1 K respectively, with a 95 % level of confidence (k = 2).

The isobaric heat capacity was measured by calorimetry using two specially designed stainless-steel vessels to prevent the presence of any vapor phase. The heat capacity of samples was measured using step method. To take the measurements, the measuring vessel was sequentially filled with a vacuum, water, and sample, while the reference vessel was maintained under vacuum (while the heating rate was 0.3 $K.min^{-1}$). The experimental setup and procedure have been previously detailed in reference [34]. Fig. 5 presents the specific heat capacity data for

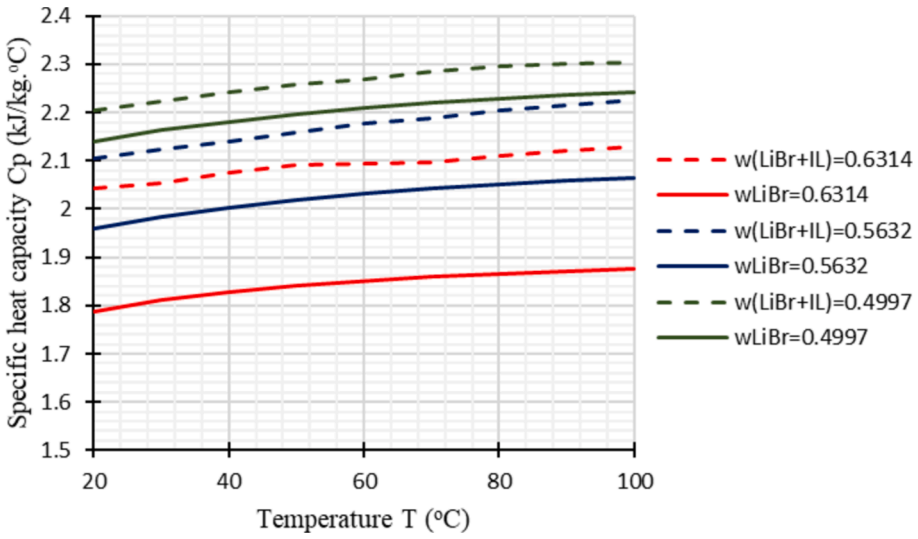


**Fig. 5.** Specific heat capacity of $H_2O$–(LiBr + [DMIM][Cl]) and $H_2O$-LiBr at different temperatures and absorbent concentrations.

absorbent mass fractions from 49.97 % to 63.14 % corresponding to solution temperatures from 20 °C to 100 °C. It can be observed from the figure that the specific heat capacity of $H_2O$–(LiBr + [DMIM][Cl]) is more as compared to $H_2O$-LiBr. Additionally, the deviation between the two working solutions is more at higher mass fraction as compared to lower mass fraction. For instance, it is 13 % and 3 % higher on average at 63.14 % and 49.97 % mass fraction respectively. The uncertainty was estimated as 0.034 J/(g·°C) for the heat capacity and 0.01 K for the temperature.

### 2.3. Absorption chiller experimental prototype and experimental conditions

The tested prototype is a 2-kW single-stage bi-adiabatic absorption chiller integrating 3D-printed adiabatic sorption exchangers (i.e., the absorber and the desorber) designed and patented by Altamirano Cundapí et al. [31]. In the desorption mode, the adiabatic sorption exchanger was characterized and demonstrated a mass effectiveness higher than 90 % at the nominal machine operating conditions [38]. The

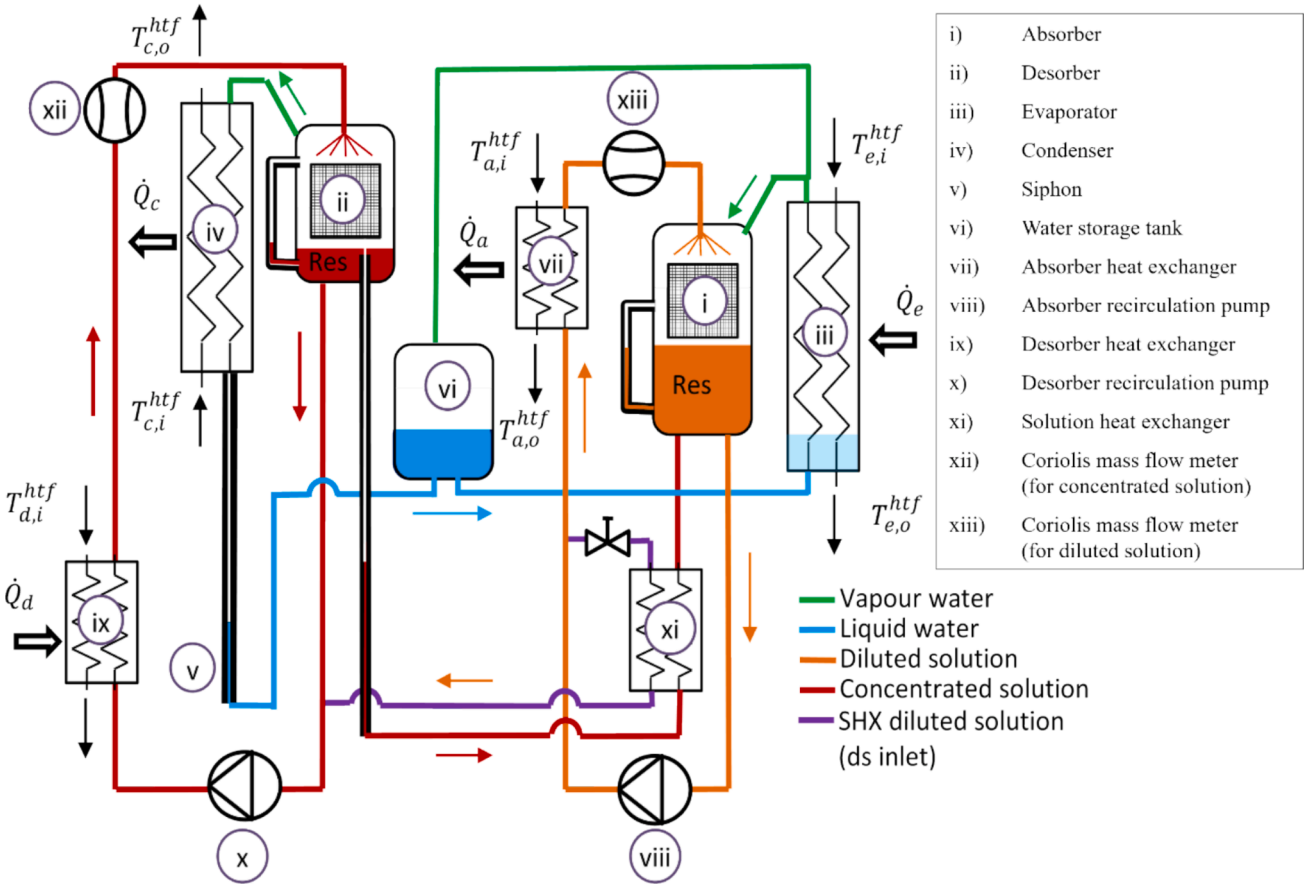


**Fig. 6.** Schematic diagram of the studied single-stage absorption chiller.

detailed description of the absorption chiller operation and its parametric global and component's characterization will be presented in a separate article. The main components of this system include an absorber heat exchanger (vii), an adiabatic absorber (i), a desorber heat exchanger (ix), an adiabatic desorber (ii), an evaporator (iii), a condenser (iv), a solution heat exchanger (xi), a siphon (v) and a water storage tank (vi). The main specificity of this prototype is that it uses commercially available plate heat exchangers (PHEs) for the heat transfers and 3D-printed adiabatic sorption exchangers for the mass transfers (i.e., the desorption and the absorption). The detailed schematic diagram of the prototype is presented in Fig. 6. The prototype operates as follows: the desorber heat exchanger (ix) heats up the solution ($\dot{Q}_d$) coming from the desorber recirculation pump (x), the superheated solution entering the adiabatic desorber (ii) generates then water vapor that flows to the condenser (iv), where it is liquefied; the heat released during condensation ($\dot{Q}_c$) is transferred to a cooling water source. The condensate is transferred from the condenser to the evaporator (iii) via a siphon (v) that is used to absorb the pressure difference between the two internal pressure levels through liquid hydrostatic pressure. Once in the evaporator, water undergoes phase change producing a cooling effect ($\dot{Q}_e$) on the cold source. The generated vapor flows then to the adiabatic absorber (i) where it is absorbed by a solution that has been previously subcooled ($\dot{Q}_a$) in the absorber heat exchanger (vii) and that is circulated thanks to the absorber recirculation pump (viii). This pump is also used to send a part of the diluted solution to the desorber, where the cycle starts again. On the way from the absorber to the desorber, the solution passes through an internal heat recovery device (solution heat exchanger, (xi)) which pre-heats it and pre-cools the solution coming from the desorber to the absorber.

A 7-kW electric resistance is used as a high temperature source, the intermediate temperature that links the absorber and the condenser in a parallel configuration is maintained at the desired temperature by means of a heat exchanger supplied with tap water; finally, a 3-kW thermostatic bath is used as the cold source. A water storage tank (vi), connected to the evaporator is used to absorb the solution concentration variations (impacting its water content) in the system. The free surface level in the evaporator is fixed by the amount of water within the water tank, On the other hand, the chamber of the adiabatic absorber (i) is used as a solution storage tank to absorb the concentration variations. The solution level in the adiabatic desorber chamber is kept constant thanks to an overflow. Regarding the instrumentation, PT100 temperature probes are used to measure the temperature at all the desired locations, whereas Coriolis mass flow meters are used to determine the concentration and flow rate of the diluted and concentrated solutions before entering the adiabatic absorber and desorber, respectively. Capacitive pressure sensors are placed at the top of adiabatic absorber and desorber tanks to measure the high and low operating pressures. Finally, magnetic flow meters are used to measure the flow rate of the external heat transfer fluid (HTF) circuits (desorber heat exchanger, absorber heat exchanger, condenser, and evaporator). Regarding the data acquisition, an Agilent 34972A data acquisition system is used coupled with a LabVIEW user interface to collect and display in real time the sensors data with an acquisition frequency of 0.1 Hz.

The experimental conditions used in the present study are shown in Table 1. The testing facility allows the independent control of all inlet variables, enabling to compare the performance of $H_2O$-LiBr and $H_2O$–(LiBr + [DMIM][Cl]) solutions. During experiments, the steady-state condition is assumed to be reached after 30 min of constant independent variables. For the data presented in this work, at least 5 min of averaged data was used for every steady-state condition. As an example, the Fig. 7 shows the temperature of heat transfer fluid at inlet and outlet position of the adiabatic absorber as a function of time at $T_{d,i}^{htf} = 100^{\circ}C$ and $T_{e,i}^{htf} = 9^{\circ}C$, for the case of IL. After 20 min, the curve stabilizes with only a minor deviation, which is within the temperature sensor's uncertainty of 0.1 °C. To ensure that all other variables (including internal and external circuit variables) also reach a steady state, a duration of 30 min was typically chosen. This criterion was consistently applied to all other variables.

**Table 1**
Operating conditions.

| | |
|---|---|
| Driving temperature at the desorber heat exchanger | 90 °C, 100 °C |
| Cold source inlet temperature at evaporator | 9 °C – 25 °C |
| Intermediate temperature source (inlet of condenser and absorber) | 25 °C |
| Absorber heat exchanger HTF flow rate | 8 lpm |
| Condenser HTF flow rate | 7 lpm |
| Desorber heat exchanger HTF flow rate | 8 lpm |
| Evaporator HTF flow rate | 7 lpm |

### 2.4. Data calculation

The measured variables allow to calculate the parameters needed to compare the performance of $H_2O$-LiBr and $H_2O$–(LiBr + [DMIM][Cl]) solutions in the absorption chiller prototype. These parameters are described in Eqs. (1)-(9) for the desorber heat exchanger heat load, absorber heat exchanger heat load, condenser heat load, evaporator heat load, solution heat exchanger heat load, thermal COP, and heat exchanger effectiveness, respectively.

$$\dot{Q}_d = \dot{m}_d^{htf} c_p^{EG} (T_{d,i}^{htf} - T_{d,o}^{htf}) \quad (1)$$

$$\dot{Q}_a = \dot{m}_a^{htf} c_p^{wt} (T_{a,o}^{htf} - T_{a,i}^{htf}) \quad (2)$$

$$\dot{Q}_c = \dot{m}_c^{htf} c_p^{wt} (T_{c,o}^{htf} - T_{c,i}^{htf}) \quad (3)$$

$$\dot{Q}_e = \dot{m}_e^{htf} c_p^{wt} (T_{e,i}^{htf} - T_{e,o}^{htf}) \quad (4)$$

$$\dot{Q}_{shx} = \dot{m}_{shx}^{d.sol} c_p^{d.sol} (T_o^{d.sol} - T_i^{d.sol}) \quad (5)$$

$$COP_{th} = \frac{\dot{Q}_e}{\dot{Q}_d} \quad (6)$$

$$\varepsilon = \dot{Q}_{act} / \dot{Q}_{max} \quad (7)$$

Where

$$\dot{Q}_{act} = C_{hot}(T_{hot,i} - T_{hot,o}) or C_{cold}(T_{cold,o} - T_{cold,i}) \quad (8)$$

$$\dot{Q}_{max} = C_{min}(\Delta T_{max}) \quad (9)$$

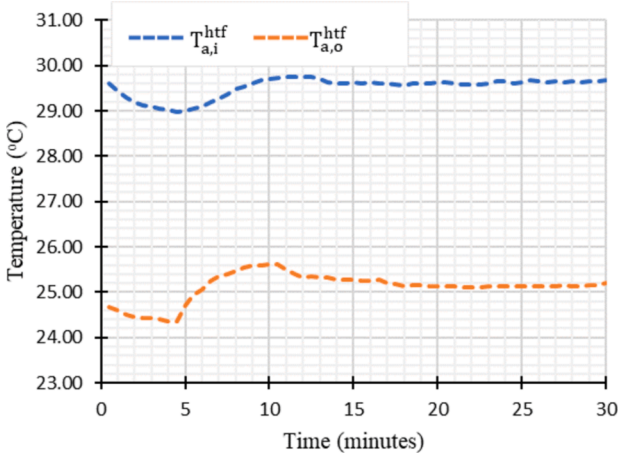


**Fig. 7.** Temperature as a function of time to reach steady state conditions.

Where C is the heat capacity rate of the fluid

## 3. Uncertainty analysis

The experimental setup is instrumented in order to evaluate the temperature, pressure, flow rates and solution concentration at multiple point of the cycle. The pressure sensors (Pfeiffer Vacuum CPT 200) have an accuracy of ± 0.2 %. The Coriolis flow meters have a precision of ± 0.1 % on the flow rate and density of the fluid. The temperature sensors (PT100) have a precision of ± 0.1 °C. The uncertainty of Krohne AF- E 400 magnetic flow meter was ± 0.2 % full scale. The Root Sum Square (RSS) method, which is a statistical technique, has been used to evaluate the combined uncertainty in parameters dependent on independent variables, each with its own uncertainty. First, the individual uncertainties of the independent variables were identified and squared. Then, the squared uncertainties were summed, and the square root of this total was taken. This results in the combined uncertainty for each parameter. Table 2 presents the uncertainty in each calculated parameter resulting from the uncertainty in the measured variables. The uncertainty at each point is shown in the plots in section 4 in the form of error bars (in positive and negative directions).

## 4. Results and discussion

In this section, the results are presented and discussed to study the effect of [DMIM][Cl] as additive in $H_2O$-LiBr on the performance of a single-stage absorption chiller prototype. The fundamental benefit of utilizing [DMIM][Cl] as additive, relies on the enhanced solubility of the resulting solution. The impact of [DMIM][Cl] additives on machine performance are presented in the form of comparison of thermal COP, heat loads and thermal effectiveness for heat transfer components.

### 4.1. Improvement in solubility

The solid–liquid equilibrium is illustrated in Fig. 8 in the absorbent mass fraction range of 0.58 to 0.69 for $H_2O$-LiBr and $H_2O$–(LiBr + [DMIM][Cl]) [34 35] (where [DMIM][Cl] mass fraction is 6 % in the absorbent (LiBr + [DMIM][Cl]). Beneath each crystallization line, the solution contains solid salt, while above them, only a liquid phase is present. As anticipated, increased temperature results in a greater capacity for salt to dissolve. In absorption refrigeration and heat pumps, the exit of SHX rich in absorbent (which is linked to absorber inlet) is the zone with the highest risk of LiBr crystallization. From Fig. 8, one can observe an average decrease of 16 °C in crystallization temperature for $H_2O$–(LiBr + [DMIM][Cl]) in an absorbent mass fraction range between 0.60 and 0.65. A decrease of 15 °C in crystallization temperature was found for $H_2O$–(LiBr + [DMIM][Cl]) compared to $H_2O$-LiBr at an absorbent mass of 65 %. This clearly shows the potential benefit of adding [DMIM][Cl] in $H_2O$-LiBr as it considerably improves the solubility of the saline solution and can provide a greater safety buffer against crystallization. The improvement in solubility can allow the absorption chillers to better operate as air-cooled system (eliminating the need of a direct-contact cooling tower) and as a heat pump for heating purposes (where the LiBr concentration needs to be higher).

The improvement in solubility that was measured through the visual-polythermal method by the CREVER Research Group was experimentally validated by the present study with the experimental absorption prototype. In Fig. 8, the concentration and temperature of the diluted solution at the inlet of the SHX are plotted for both studied working fluids. Most of the points are above the crystallization line; however, crystallization is observed for $H_2O$-LiBr at the highest driving temperature and lowest cold source inlet temperature ($T_{d,i}^{htf} = 100^{\circ}C$ and $T_{e,i}^{htf} = 9^{\circ}C$, respectively), which lead to the highest absorbent concentration (0.624) at a solution temperature of 29 °C. The crystallization phenomenon impeded the operation of the absorption prototype and therefore, the results for this steady-state operating condition is missing (Figs. 6-12). For $H_2O$–(LiBr + [DMIM][Cl]), however, no crystallization was observed at similar operating conditions (solution temperature of 29.4 °C with an absorbent concentration of 0.626). From this, one can observe that the working fluid with the additive was able to operate in concentration and temperature ranges that otherwise would be impossible (due to crystallization) with the conventional $H_2O$-LiBr working fluid and therefore, the effectiveness of using [DMIM][Cl] as anti-crystallization additive in absorption chillers is demonstrated.

### 4.2. Absorber

The absorber heat load as a function of the inlet evaporator temperature is presented in Fig. 9 showing an increasing trend. The studied machine links a plate heat exchanger, where heat transfers take place, to an adiabatic absorber, where mass transfers take place. The thermal load mentioned here concerns the heat transfer within the exchanger, which indirectly reflects the efficiency of the mass transfer within the adiabatic absorber. For the case of $T_{d,i}^{htf} = 90^{\circ}C$, $H_2O$-LiBr and $H_2O$–(LiBr + [DMIM][Cl]) exhibit remarkably similar performances at high inlet evaporator temperatures (e.g., a relative difference of around 1 % for $T_{e,i}^{htf} = 25^{\circ}C$). While at low inlet evaporator temperatures, the absorber heat load of $H_2O$–(LiBr + [DMIM][Cl]) is higher than that of $H_2O$-LiBr (e.g., a 8 % relative difference at $T_{e,i}^{htf} = 13^{\circ}C$). On the other hand, for $T_{d,i}^{htf} = 100^{\circ}C$, the absorber heat load for $H_2O$–(LiBr + [DMIM][Cl]) is higher than that of $H_2O$-LiBr. This difference is more prominent at lower inlet evaporator temperatures (reaching a maximum of up to 34 % at $T_{e,i}^{htf} = 13^{\circ}C$), while it decreases at high inlet evaporator temperatures (e.g., around 1 % at $T_{e,i}^{htf} = 25^{\circ}C$). This indicates that high absorbent concentrations (low evaporator temperatures and high desorber temperatures) lead to improved absorber heat loads for $H_2O$–(LiBr + [DMIM][Cl]) compared with $H_2O$-LiBr. An explanation to this might be related to the lower viscosity and higher specific heat capacity of the solution with the additive with respect to that of $H_2O$-LiBr, especially at high absorbent concentrations (see Fig. 4 and Fig. 5). Indeed, a lower viscosity can decrease the falling film thickness and increase the mass diffusivity of the solution in the adiabatic absorber (reducing the mass transfer resistance), leading to an enhanced water vapor absorption and a lower solution concentration at the absorber heat exchanger. In an adiabatic absorber, heat exchange occurs separately, so the higher specific heat capacity solution means have higher enthalpy, which can lead to an increased absorber heat load. Other parameters that might be impacted by the addition of the additive and that could play an important role in absorption enhancement includes the properties affecting heat and mass transfer (i.e., mass diffusivity). Indeed, this aspect will need to be further investigated in future studies.

From Fig. 9, one can observe that the data point for the conventional

**Table 2**
Uncertainties in calculated parameters.

| Uncertainty in calculated parameters | Maximum Absolute Uncertainty |
|---|---|
| Uncertainty in heat loads $U(\dot{Q}) = \sqrt{(\frac{\delta\dot{Q}}{\delta\dot{m}}u_{\dot{m}})^2 + (\frac{\delta\dot{Q}}{\delta T_i}u_{T_i})^2 + (\frac{\delta\dot{Q}}{\delta T_o}u_{T_o})^2}$ | $U(\dot{Q}_a) = 0.09$, $U(\dot{Q}_d) = 0.11$, $U(\dot{Q}_c) = 0.093$, $U(\dot{Q}_e) = 0.077$ |
| Uncertainty in thermal COP $U(COP_{th}) = \sqrt{(\frac{\delta COP_{th}}{\delta\dot{Q}_d}u_{\dot{Q}_d})^2 + (\frac{\delta COP_{th}}{\delta\dot{Q}_e}u_{\dot{Q}_e})^2}$ | $U(COP_{th}) = 0.027$ |
| Uncertainty in thermal effectiveness $U(\varepsilon) = \sqrt{(\frac{\delta\varepsilon}{\delta\dot{Q}_{max}}u_{\dot{Q}_{max}})^2 + (\frac{\delta\varepsilon}{\delta\dot{Q}_{act}}u_{\dot{Q}_{act}})^2}$ | $U(\varepsilon_a) = 0.05$, $U(\varepsilon_d) = 0.06$, $U(\varepsilon_c) = 0.054$, $U(\varepsilon_e) = 0.058$ |

Where U represents the Uncertainty in calculated parameters, while u represents the uncertainty in individual variables

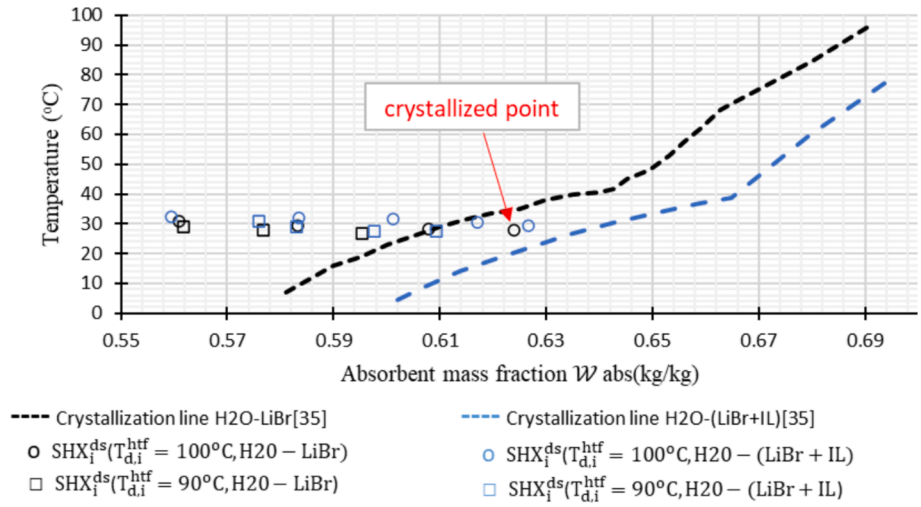


**Fig. 8.** Solid-liquid equilibrium curves of $H_2O$-LiBr and $H_2O$–(LiBr + [DMIM][Cl]) solutions [35] and diluted solution conditions at the inlet of the SHX during the experimental campaign in the absorption chiller prototype.

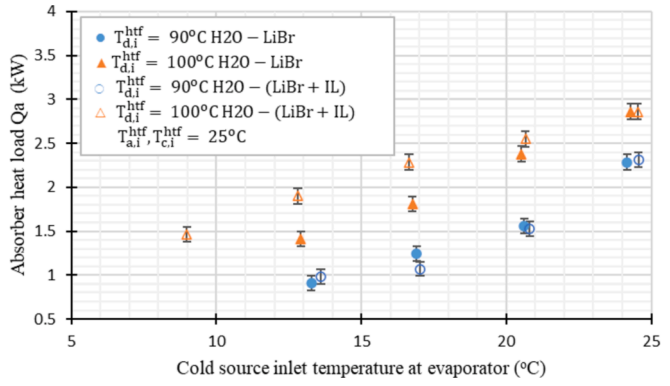


**Fig. 9.** Absorber heat load as a function of the inlet evaporator temperature.

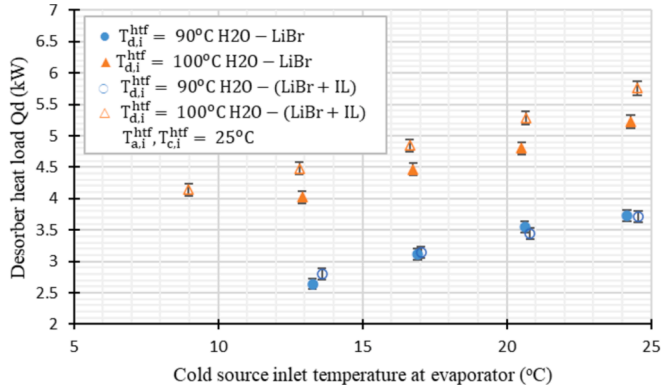


**Fig. 10.** Desorber heat exchanger load as a function of the inlet evaporator temperature.

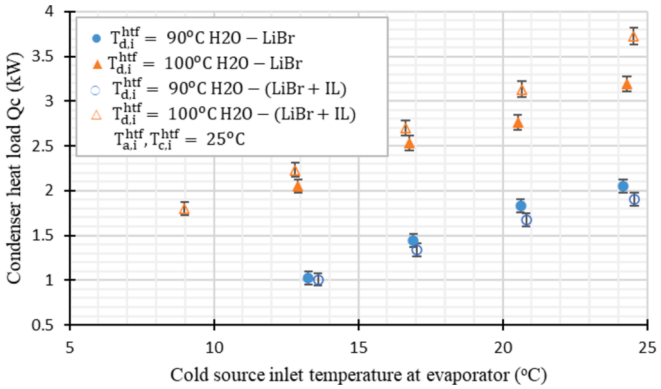


**Fig. 11.** Condenser heat load as a function of the inlet evaporator temperature.

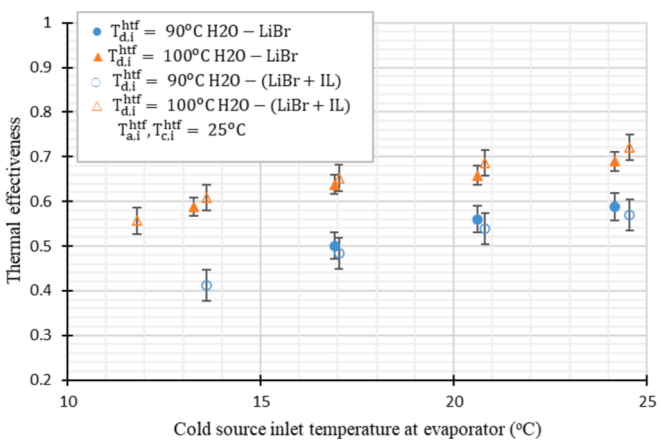


**Fig. 12.** Condenser heat exchanger thermal effectiveness as a function of the inlet evaporator temperature.

working fluid (without IL) at a driving temperature of 100 °C and the lowest inlet evaporator temperature (9 °C) is missing due to crystallization at this condition. This inlet evaporator temperature is close to the nominal chilled water temperature of commercial $H_2O$-LiBr chillers (between 7 and 15 °C) [7]. The presented prototype faces a crystallization risk at this operating condition, where commercial chillers typically do not, due to two main reasons: the low effectiveness of the presented prototype evaporator (see Fig. 14) increases the temperature pinch which can result in lower operating pressure in evaporator and consequently in absorber as compared to commercial chillers. The other reason is the prototype's architecture, which, in adiabatic absorption, leads to higher concentrations of the solution in the solution circuit.

### 4.3. Desorber

The desorber heat load as function of the inlet evaporator temperature is shown in Fig. 10. As expected, the desorber heat load increases as the driving temperature increases from 90 °C to 100 °C, since higher driving temperatures increase the desorption potential, increasing the circulated refrigerant fluid and the heat loads at the different heat transfer components. Results show that the desorber heat load for $H_2O$-LiBr is marginally above with less than 3 % difference as compared with $H_2O$–(LiBr + [DMIM][Cl]) at $T_{d,i}^{htf} = 90^{\circ}$. The exception is found at $T_{e,i}^{htf} = 13^{\circ}$, where the heat load for $H_2O$–(LiBr + [DMIM][Cl]) is 6 % higher as compared to $H_2O$-LiBr. For the case of $T_{d,i}^{htf} = 100^{\circ}$, the desorber heat load for $H_2O$–(LiBr + [DMIM][Cl]) is higher (up to 11 %) in comparison with $H_2O$-LiBr. Higher desorber heat load values might be related to the enhanced desorption phenomenon linked to the theoretical cycle obtained thanks to the higher equilibrium vapor pressure of $H_2O$–(LiBr + IL) (see Fig. 2) as compared with $H_2O$-LiBr. This means that for the same operating pressure (set out by the condenser temperature), the working fluid with the additive has the theoretical potential to reach a higher concentration (in absorbent). Hence, more refrigerant vapor can be desorbed with the same driving temperature. Another explanation for this might be related to higher specific heat capacity of the solution with the additive as compared to $H_2O$-LiBr (see Fig. 5). Higher specific heat capacity solution results in higher heat load as more energy will be required to reach the desired desorption. From Fig. 10, one can observe that this phenomenon is less evident at lower absorbent concentrations (90 °C driving temperature), for which the desorber heat loads are remarkably close for both solutions.

### 4.4. Condenser

The heat load at the condenser as a function of the inlet evaporator temperature is shown in Fig. 11. The condenser heat load increases with both $T_{e,i}^{htf}$ and $T_{d,i}^{htf}$. As discussed in section 4.3, the increased driving temperature increases the refrigerant desorption rate at the desorber. Consequently, the condenser load increases as the refrigerant flow rate increases. At $T_{d,i}^{htf} = 90^{\circ}$C, the condenser heat load for $H_2O$–(LiBr + IL) is slightly lower as compared with $H_2O$-LiBr (a relative difference in the range of 2–8 %). On the other hand, for the case of $T_{d,i}^{htf} = 100^{\circ}$C, the condenser heat load is higher for the solution containing [DMIM][Cl] with a relative difference that is low (8 %) at low $T_{e,i}^{htf}$ and increases up to 17 % for $T_{e,i}^{htf} = 25^{\circ}C$. The reason behind this might be explained by the same phenomenon happening in the desorber; i.e., as discussed in section 4.3, an increased desorption potential of the solution due to an increased equilibrium vapor pressure. The higher refrigerant mass flow rate generated by the solution with the additive ends up flowing to the condenser, where higher heat loads are required.

The thermal effectiveness of the condenser as a function of the inlet evaporator temperature is shown in Fig. 12. The thermal effectiveness increases with both $T_{e,i}^{htf}$ and $T_{d,i}^{htf}$, which is directly related to condenser heat load. Indeed, the effectiveness of the exchanger increases with the refrigerant flow rate, which is a normal behavior in the turbulent regime [39]. The thermal effectiveness for $H_2O$-LiBr is 0.55 and 0.64 on average at driving temperatures of 90 °C and 100 °C, respectively. Whereas, for $H_2O$–(LiBr + [DMIM][Cl]), the thermal effectiveness is 0.53 and 0.64 on average for the same conditions, respectively. The performance of the condenser with both solutions is similar (as expected) with a relative difference of less than 4 % at 90 °C and 100 °C driving temperatures.

### 4.5. Evaporator

The cooling capacity as a function of the inlet evaporator temperature is shown in Fig. 13. As observed, it increases with both $T_{e,i}^{htf}$ and $T_{d,i}^{htf}$.

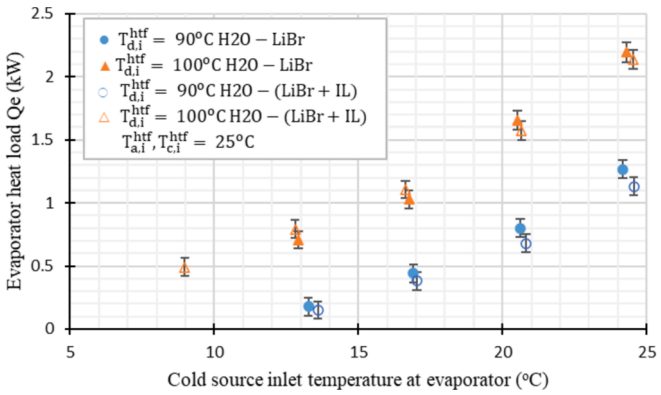


**Fig. 13.** Cooling capacity as a function of the inlet evaporator temperature.

Indeed, increasing the driving temperature results in an increase of thrust, meaning that more thermal energy is available to drive the absorption process, facilitating the desorption of the refrigerant from the absorbent solution. Consequently, this enables the generation of more cooling capacity in the evaporator. In the case of $T_{d,i}^{htf} = 90^{\circ}C$, the cooling capacity for the conventional working fluid is higher (up to 15 %) in comparison with that of the solution with IL, especially at low $T_{e,i}^{htf}$. Whereas in the case of $T_{d,i}^{htf} = 100^{\circ}C$, the cooling capacity of $H_2O$–(LiBr + [DMIM][Cl]) is lower at high values of $T_{e,i}^{htf}$ (e.g., it is 8 % lower at $T_{e,i}^{htf} = 25^{\circ}C$), but higher at low $T_{e,i}^{htf}$ (e.g., it is 12 % higher at $T_{e,i}^{htf} = 13^{\circ}C$). This might can be explained by the uncertainty in the measurements. According to the phenomena observed at the different components, the evaporator heat load should be systematically higher at high driving temperatures, which is not the case. The reason behind this might be related to the specific design of the prototype. Indeed, as mentioned in section 2.3, the evaporator's level is regulated through the water storage tank (which is connected in parallel). Therefore, at lower solution concentrations (higher evaporating temperatures), the water level in the evaporator is lower, which might have an impact on the available exchange surface for evaporation, limiting its performances and leading to the poorer results of the evaporator load at these conditions.

The evaporator thermal effectiveness as a function of the inlet evaporator temperature is shown in Fig. 14. This effectiveness is 0.35 and 0.40 on average for the $H_2O$-LiBr solution at driving temperatures of 90 °C and 100 °C, respectively. For the case of $H_2O$–([DMIM][Cl] + LiBr), the thermal effectiveness is 0.39 and 0.41 on average for the same conditions, respectively. The average difference at 90 °C and 100 °C of

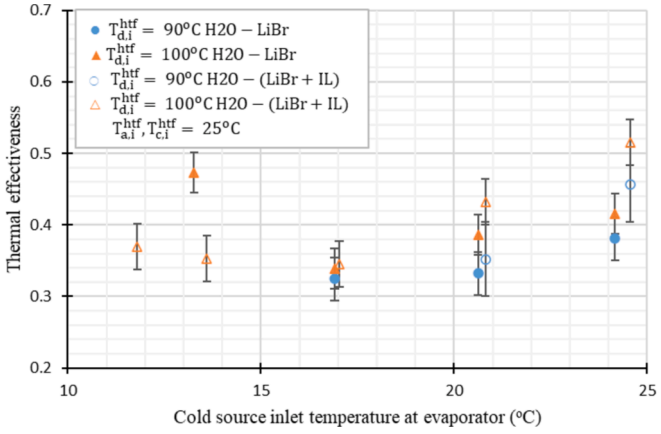


**Fig. 14.** Evaporator thermal effectiveness as a function of the inlet evaporator temperature.

driving temperature is small, which depicts the same performance of both working fluids. A small difference at a driving temperature of 100 °C is however observed typically at lower evaporator temperature. This difference can be attributed to the experimental uncertainties.

### 4.6. Thermal COP

The thermal COP as a function of the inlet evaporator temperature is presented in Fig. 15. The COP values of this prototype are significantly lower than the nominal ones of commercial $H_2O$-LiBr absorption chillers, which typically range from 0.6 to 0.8) [7]. This discrepancy might be explained by the low effectiveness of the evaporator, which was designed for a nominal effectiveness of 0.8 using existing data from the literature on a single plate [40]. However, other phenomena are involved when using multiple plates in a commercial PHE. This matter, along with the performance evaluation of this prototype and its various elements using $H_2O$-LiBr under different operating conditions, will be addressed in a separate article.

From Fig. 15, one can observe that increasing $T_{e,i}^{htf}$ leads to an increase of the thermal COP for both solutions. At a driving temperature of 90 °C, the thermal COP for $H_2O$-LiBr remains higher when compared to that of $H_2O$–(LiBr + IL), with an absolute difference that increases at higher inlet evaporator temperatures (0.01 at $T_{e,i}^{htf} = 13^{\circ}C$ and 0.03 at $T_{e,i}^{htf} = 25^{\circ}C$). For $T_{d,i}^{htf} = 100^{\circ}C$ (leading to higher solution concentrations), the thermal COP of both solutions is nearly identical, with a relative difference of less than a 1 % at low inlet evaporator temperatures. At higher inlet evaporator temperature at a driving temperature of 100 °C, however, the thermal COP of $H_2O$-LiBr is up to 17 % higher than that of $H_2O$–(LiBr + IL). This discrepancy is attributed to the lower solution recirculation ratio in the desorber for the IL-containing solution compared to non-IL-containing solution. The recirculation ratio for absorber/desorber in the presented prototype is the ratio between the mass flow rate of the solution exchanged between the desorber and the absorber, and the mass flow rate of the solution recirculating in the adiabatic absorber and desorber. A possible reason for the lower recirculation ratio in the desorber is a minor disturbance in the ball valve located in the solution line. Consequently, an increase in the mass flow rate of the solution in the economiser leads to an increase in the heat rate in the desorber heat exchanger for the same cold production, resulting in a lower thermal COP at these operating points for the solution containing IL. Therefore, it is to note that this discrepancy is not related to the properties of the new solution. In addition, in this research we chose to implement IL additives in $H_2O$-LiBr in a prototype absorption chiller because we wanted to examine the effect of the additives on each component of the machine. This approach allowed us to gather detailed information on every component, which would not have been possible with a commercial chiller.

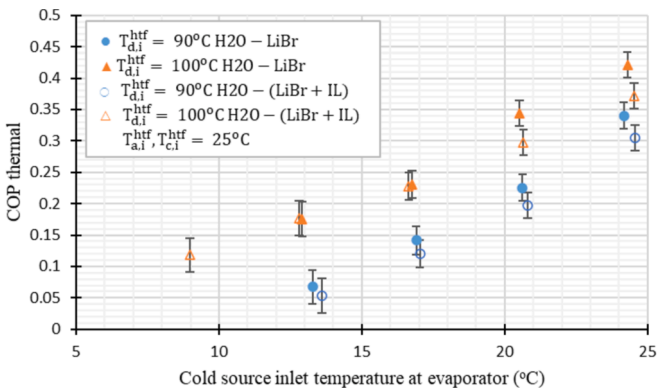


**Fig. 15.** Thermal COP as a function of the inlet evaporator temperature.

## 5. Conclusion

Absorption chillers are attractive because they utilize natural refrigerants and can be driven by waste heat or low-grade heat sources. The water-lithium bromide ($H_2O$-LiBr) working fluid is preferred because water (used as refrigerant) is abundant, non-toxic, and inexpensive. However, the inherent crystallization issue of LiBr at high concentrations limits the operating range of this technology, restricting its use as air-cooled systems or heat pumps for space heating. Furthermore, air-cooled systems offer several benefits including reduced maintenance, lower operating costs and a compact size by eliminating the cooling tower requirement. To increase this operating range, additives can be added to $H_2O$-LiBr to improve solubility and decrease crystallization risks. However, several tested additives have significant drawbacks, such as considerable reduction in heat and mass transfer and the requirement of a rectifier. To overcome these drawbacks, this work experimentally studies the effect of the ionic liquid [DMIM][Cl] as additive in $H_2O$-LiBr on the performance of a single-stage bi-adiabatic absorption chiller. The working fluid operated smoothly throughout the entire experimental domain. Furthermore, the chemical and thermal stability of the IL allows it to function across a wide range of operating conditions.

The results show that the absorber heat load for both solutions perform similar with exception to some points at $T_{d,i}^{htf} = 100^{\circ}C$ and low evaporator temperatures. Regarding the desorber, its heat load is higher (up to 11 %) for $H_2O$–(LiBr + IL) at $T_{d,i}^{htf} = 100^{\circ}C$, whereas both solutions exhibit similar performance at $T_{d,i}^{htf} = 90^{\circ}C$. Regarding the phase-change exchangers (i.e., the condenser and the evaporator), the condenser heat load is higher for $H_2O$–(LiBr + IL) at $T_{d,i}^{htf} = 100^{\circ}C$ and $H_2O$-LiBr at $T_{d,i}^{htf} = 90^{\circ}C$, respectively. The cooling capacity of both the solutions $H_2O$–(LiBr + IL) and $H_2O$-LiBr is also found very close to each other at both driving temperatures (100 °C and 90 °C). Finally, the thermal COP is similar for both working fluids, except at higher inlet evaporator temperature with a driving temperature of 100 °C. A slightly lower recirculation ratio at the desorber side for IL containing solution was the reason behind this discrepancy.

In the current experimental campaign, the improvement in solubility that was previously measured through the visual-polythermal method was experimentally validated. Indeed, crystallization (complete blockage of the solution) was identified at the SHX with $H_2O$-LiBr at $T_{d,i}^{htf} = 100^{\circ}C$ (the highest driving temperature) and the lowest evaporator temperature ($T_{e,i}^{htf} = 9^{\circ}C$), for an absorbent concentration of 0.624 at a solution temperature of 29 °C. For $H_2O$–(LiBr + [DMIM][Cl]), however, no crystallization was observed at similar operating conditions (solution temperature of 29.4 °C with an absorbent concentration of 0.626). Results show the potential of using [DMIM][Cl] as anti-crystallization additive in $H_2O$-LiBr. Even though crystallization risk still exists (causing system failure) at very high absorbent concentrations and low temperatures, depending upon the operating conditions. The addition of the proposed additive is beneficial for absorption chillers that require an extended temperature range, typically for air-cooled systems and heat pumps used for heating purposes. The anti-crystallization effect is achieved with a negligible impact on the cooling capacity and thermal COP, and without common problems associated with additives for the same purpose, such as the requirement of a rectifier and adverse effect on heat and mass transfer. Future work on $H_2O$–(LiBr + IL) will focus on further implementing this additive in a real residential or commercial application. Additionally, the molecular level investigation and heat flow associated with phase transitions of the solutions can be studied in future to provide more information about the expected improvement of new solution with additive compared to conventional $H_2O$-LiBr. Further investigation is needed to study the effects of undercooling and solid phase composition on the solid–liquid equilibrium of the new solution to provide valuable insights of

crystallization processes. Additional studies are also necessary at higher absorber and condenser cooling water temperatures to evaluate the impact of crystallization under those operating conditions. The effects of corrosion and economic considerations of new solution are important factors for practical applications which need to be addressed in future research.

## Declaration of competing interest

The authors declare that they have no known competing financial interests or personal relationships that could have appeared to influence the work reported in this paper.

## Acknowledgements

This study is part of project "PID2020-119004RB-C21", financed by Spanish Ministry MCIN/AEI/10.13039/501100011033/ and received funding from European Union's Horizon 2020 research and innovation program under the Marie Skłodowska-Curie grant agreement No. 945413 and from the Universitat Rovira i Virgili.

The authors also want to acknowledge YTC America for their funding regarding the measurements of properties of the ([DMIM][Cl] + LiBr)/water solution. We also want to acknowledge Daniel Salavera for measuring the properties of ([DMIM][Cl] + LiBr)/water solution.

## Data availability

Data will be made available on request.

## References

[1] " International Energy Agency (IEA). Annual Report, Solar Heating and Cooling Programme; International Energy Agency,", France, Paris, 2018, p. 2019.
[2] "The Future of Cooling: Opportunities for Energy-Efficient Air Conditioning," *IEA, Paris, France,* 2018.
[3] D. Mugnier, D. Neyer and S. White, The Solar Cooling Design Guide: Case Studies of Successful Solar Air Conditioning Design, Ernst & Sohn, Wiley, 2017, 978-3-433-60684-1.
[4] J. García-Domínguez, A. Blanco-Marigorta, J. Marcos, Analysis of a solar driven ORC-absorption based CCHP system from a novel exergy approach, Energ Conver Manage:x 19 (2023) 100402.
[5] N. Ibrahim, S. Rehman, F. Al-Sulaiman and F. Ani, "A systematic thermodynamic performance assessment of a solar-driven double-effect absorption chiller integrated with absorption energy storage," *Appl. Therm. Eng.,* vol. 221, no. 119868, 2023.
[6] Y. Zhou, L. Pan, X. Han and L. Sun, "Dynamic modeling and thermodynamic analysis of lithium bromide absorption refrigeration system using Modelica," *Appl. Therm. Eng.,* vol. 225, no. 120106, 2023.
[7] A. Altamirano, N. Pierrès, B. Stutz, Review of small-capacity single-stage continuous absorption systems operating on binary working fluids for cooling: Theoretical, experimental and commercial cycles, Int. J. Refrig. 106 (2019) 350–373, https://doi.org/10.1016/j.ijrefrig.2019.06.033.
[8] N. Mirl, F. Schmid, B. Bierling, K. Spindler, Design and analysis of an ammonia-water absorption heat pump, Appl. Therm. Eng. 165 (2020) 114531, https://doi.org/10.1016/j.applthermaleng.2019.114531.
[9] S. Braccio, H. Phan, M. Wirtz, N. Tauveron, N. Pierres, Simulation of an ammonia-water absorption cycle using exchanger effectiveness, Appl. Therm. Eng. 213 (2022) 118712, https://doi.org/10.1016/j.applthermaleng.2022.118712.
[10] "NewYork State," [Online]. Available: https://www.health.ny.gov/environmental/emergency/chemical_terrorism/ammonia_general.htm. [Accessed 04 04 2023].
[11] H. Zhang, D. Yin, S. You, W. Zheng, B. Li, X. Zhang, Numerical and experimental investigation on the heat and mass transfer of falling film and droplet regimes in horizontal tubes LiBr-H2O absorber, Appl. Therm. Eng. 146 (2019) 752–767, https://doi.org/10.1016/j.applthermaleng.2018.10.046.
[12] M. Izquierdo, M. Venegas, P. Rodrıguez, A. Lecuona, Crystallization as a limit to develop solar air-cooled LiBr–H2O absorption systems using low-grade heat," *Solar Energy Mater*, Solar Cells 81 (2) (2004) 205–216, https://doi.org/10.1016/j.solmat.2003.11.002.
[13] X. Liao, R. Radermacher, Absorption chiller crystallization control strategies for integrated cooling heating and power systems, Int. J. Refrig. 30 (2007) 904–911, https://doi.org/10.1016/j.ijrefrig.2006.10.009.
[14] R. Reimann, "Properties of the Carrol System and a Machine Design for Solar Powered, Air Cooled, Absorption Space Cooling," *Report No. DOE/CS/31587-T2,* 1981.
[15] N. Inoue, H2O/LiBr+C2H2(OH)2 system and H2O/LiBr+ZnCl2 system, Reito (japan) 68 (1993) 719–723.
[16] Y. Park, J. Kim, H. Lee, Physical properties of the lithium bromide+1,3-propanediol+water system, Int. J Refrig. 20 (5) (1997) 319–325, https://doi.org/10.1016/S0140-7007(97)00021-2.
[17] J. Kim, Y. Park, H. Lee, Performance evaluation of absorption chiller using LiBr+H2N(CH2)2OH+H2O, LiBr+HO(CH2)3OH+H2O and LiBr+(HOCH2CH2)2NH+H2O as working fluids, Appl. Therm. Eng. 19 (2) (1999) 217–225, https://doi.org/10.1016/S1359-4311(98)00032-5.
[18] J. Yoon, O. Kwon, Cycle analysis of air-cooled absorption chiller using a new working solution, Energy 24 (9) (1999) 795–809, https://doi.org/10.1016/S0360-5442(99)00038-9.
[19] S. Iyoki, R. Yamanaka, T. Uemura, Physical and thermal properties of the waterelithium bromideelithium nitrate system, Int. J Refrig. 16 (3) (1993) 191–200, https://doi.org/10.1016/0140-7007(93)90048-D.
[20] K. Koo, H. Lee, S. Jeong, Y. Oh, D. Park, Y. Baek, Solubilities, Vapor Pressures, and Heat Capacities of the Water + Lithium Bromide + Lithium Nitrate + Lithium Iodide + Lithium Chloride System, Int. J. Thermophys. 20 (1999) 589–600.
[21] H. Iizuka, K. Nagamatsuya, K. Takahashi and J. Kuroda, "Absorbent solution for use with absorption refrigeration apparatus". Patent U.S. Patent 5108638, 1992.
[22] K. Wang, P. Kisari, O. Abdelaziz and E. Vineyard, "Testing of crystallization temperature of a new working fluid for absorption heat pump systems," in *Proceedings of "Road to Climate Friendly Chillers: Moving Beyond CFCs and HCFCs"*, Cairo, Egypt, 2010.
[23] H. Araújo, L. Massuchetto, R. Nascimento, S. Carvalho and J. Dangelo, "Thermodynamic performance analysis of a single-effect absorption refrigeration system operating with water and 1-ethyl-3-methylimidazolium-based ionic liquids mixtures," *Appl. Therm. Eng.,* Vols. 201, Part A, p. 117761, 2022, https://doi.org/10.1016/j.applthermaleng.2021.117761.
[24] C. Zhai, Y. Sui, Z. Sui and W. Wu, "Ionic liquids for microchannel membrane-based absorption heat pumps: Performance comparison and geometry optimization," *Energy Conv Manag.,* vol. 239, no. 114213, 2021, https://doi.org/10.1016/j.enconman.2021.114213.
[25] L. Jing, Z. Danxing, F. Lihua, W. Xianhong, D. Li, Vapor Pressure Measurement of the Ternary Systems H2O + LiBr + [Dmim]Cl, H2O + LiBr + [Dmim]BF4, H2O + LiCl + [Dmim]Cl, and H2O + LiCl + [Dmim]BF4, J. Chem. Eng. Data 56 (1) (2011) 97–101, https://doi.org/10.1021/je1009202.
[26] K. Kim, D. Demberelnyamba, B. Shin, S. Yeon, S. Choi, J. Cha, H. Lee, C. Lee, J. Shim, Surface tension and viscosity of 1-butyl-3-methylimidazolium iodide and 1-butyl-3-methylimidazolium tetrafluoroborate, and solubility of lithium bromide +1-butyl-3-methylimidazolium bromide in water, Korean J. of Chem Engg. 23 (2006) 113–116, https://doi.org/10.1007/BF02705701.
[27] M. Zafarani-Moattar, F. Frouzesh, The study of vapor–liquid equilibria of 1-ethyl-3-methyl imidazolium chloride and 1-butyl-3-methyl imidazolium chloride in lithium bromide aqueous solutions and their corresponding binary systems at 298.15 K, Calphad 40 (2013) 16–23, https://doi.org/10.1016/j.calphad.2012.11.002.
[28] M. Królikowska, M. Zawadzki, M. Skonieczny, The influence of bromide-based ionic liquids on solubility of LiBr (1) + water (2) system. Experimental (solid + liquid) phase equilibrium data. Part 2, J. Molecular Liq. 265 (2018) 316–326, https://doi.org/10.1016/j.molliq.2018.06.006.
[29] M. Królikowska, T. Hofman, The influence of bromide-based ionic liquids on solubility of LiBr (1)+water (2) system. Experimental (solid + liquid) phase equilibrium data.Part 1, J. Molecular Liq. 273 (2019) 606–614, https://doi.org/10.1016/j.molliq.2018.09.104.
[30] M. Shiflett, K. Kontomaris, S. Lustig, M. Scialdone, M. Quigley, B. Mellein, Ionic compounds in lithium bromide/water absorption cycle systems, United States Patent Patent US (2012) 2012.
[31] A. S. B. L. P. N. Altamirano Cundapí, "Sorption exchanger (in French), French Patent FR 3114381 (A1). French National Institute of Industrial Property.". 2020, https://patents.google.com/patent/FR3114381A1/.
[32] L. Chunhuan, Z. Yuan, S. Qingquan, Saturated vapor pressure, crystallization temperature and corrosivity of LiBr-[BMIM]Cl/H2O working pair, CIESC Journal 67 (4) (2016) 1110–1116, https://doi.org/10.11949/j.issn.0438-1157.20150230.
[33] "Exploration of Ionic Liquids or new chemical compunds for improving efficiency of absorption chillers and as heat transfer medium for solar energy harvesting," CREVER, Research Group of Applied Thermal Engineering, URV, Tarragona, Spain, 2017.
[34] D. Salavera, X. Esteve, K. Patil, A. Mainar, A. Coronas, Solubility, Heat Capacity, and Density of Lithium Bromide + Lithium Iodide + Lithium Nitrate + Lithium Chloride Aqueous Solutions at Several Compositions and Temperatures, J. Chemical & Engg. Data 49 (3) (2004) 613–619, https://doi.org/10.1021/je034202x.
[35] D. Latorre, D. Salavera, M. Larrechi, A. Coronas, Influence of 1,3-dimethylimidazolium chloride on the solubility of lithium bromide in water for absorption refrigeration and heat pumps, En: *XI Congreso Ibérico y IX Congreso Iberoamericano de Ciencias y Técnicas del Frío Cytef2022.* Avances en Ciencias y Técnicas del Frío - 11,Universidad Politécnica de Cartagena,Cartagena, 2022, pp. 156-160, ISBN:978-84-17853-55-6, doi:10.31428/10317/11521.
[36] D. Salavera, S. Chaudhari, X. Esteve, A. Coronas, Vapor−Liquid Equilibria of Ammonia + Water + Potassium Hydroxide and Ammonia + Water + Sodium Hydroxide Solutions at Temperatures from (293.15 to 353.15) K, J. Chem. Eng. Data 50 (2) (2005) 471–476, https://doi.org/10.1021/je049708+.
[37] S. Libotean, A. Martin, D. Salavera, M. Valles, X. Esteve, A. Coronas, Densities, Viscosities, and Heat Capacities of Ammonia + Lithium Nitrate and Ammonia + Lithium Nitrate + Water Solutions between (293.15 and 353.15) K, J. Chem. Eng. Data 53 (10) (2008) 2383–2388, https://doi.org/10.1021/je8003035.

[38] A. Altamirano, B. Stutz, N. Pierrès, Experimental Characterization of a Three-Dimensional-Printed Adiabatic Desorber for Absorption Chillers, Heat Transfer Engineering 43 (22) (2022) 1867–1884, https://doi.org/10.1080/01457632.2021.2022301.

[39] T. Bergman, A. Lavine, F. Incropera and D. Dewitt, Fundamentals of Heat and Mass Transfer, JOHN WILEY & SONS, Seventh Edition.

[40] F. Giraud, "Vaporization of water at subatmospheric pressure: fundamentals of boiling phenomena and path towards the design of compact evaporators for sorption chillers," *PhD Thesis INSA Lyon,* 2015.